THE SEISMOLOGICAL SOCIETY OF AMERICA
400 Evelyn Ave., Suite 201
Albany, CA 94706-1375
(510) 525-5474; FAX (510) 525-7204
www.seismosoc.org

Acoustic Characterization of Explosion Complexity at Sakurajima, Karymsky, and Tungurahua Volcanoes

by Robin S. Matoza, David Fee, and Taryn M. López

Online Material: Figures showing normalized onset peak pressure and energy across the Sakurajima network.

INTRODUCTION

Great diversity has been observed in volcanic infrasound signals worldwide, reflecting rich variability in their physical source mechanisms. Infrasound waveforms, estimated signal powers, and frequency contents vary dramatically across a large spectrum of physical eruptive styles (e.g., Johnson and Ripepe, 2011; Fee and Matoza, 2013; Garces *et al.*, 2013). The observed infrasound signals and eruptive styles span, but do not fall neatly into, the idealized terms such as Hawaiian, Strombolian, Vulcanian, sub-Plinian, and Plinian (e.g., Walker, 1973; Fee and Matoza, 2013). In physical volcanology, the description and classification of explosive eruption styles are traditionally based on metrics of the thickness, areal extent, and grain size distributions of eruptive products (Walker, 1973). However, eruptive products represent time-integrated end results of the fragmentation, ejection, and dispersal processes, and the idealized terms do not adequately capture the observed diversity in explosion styles. Infrasound data, which represent a geophysical recording of the explosion process, show promise for better characterizing, quantifying, and classifying the many varied mechanisms and styles of explosive eruptions (e.g., Johnson, 2007; Sahetapy-Engel *et al.*, 2008; Marchetti *et al.*, 2009; Lopez *et al.*, 2013).

Previous conceptual understanding of acoustic signals from explosive eruptions has tended to focus on two end-member signal durations: (1) discrete explosion (blast) waves with relatively simple waveforms lasting from several to tens of seconds (e.g., Firstov and Kravchenko, 1996; Ripepe and Marchetti, 2002; Johnson, 2003; Marchetti *et al.*, 2009, 2013) and (2) sustained, broadband, infrasonic tremor signals lasting from minutes to hours (e.g., Vergniolle and Caplan-Auerbach, 2006; Matoza *et al.*, 2009; Fee, Steffke, and Garces, 2010; Caplan-Auerbach *et al.*, 2010). Commonly, the discrete explosion signals are simply called "explosions" in the volcano acoustics literature and they have been modeled, using linear equivalent source theory, as acoustic monopoles, that is, sources represented as time-varying mass fluxes (e.g., Woulff and McGetchin, 1976; Firstov and Kravchenko, 1996; Johnson, 2003; Delle Donne and Ripepe, 2012; Johnson and Miller, 2014). However, it is recognized that in many cases these "explosion" waves have nonlinear characteristics (Yokoo and Ishihara, 2007; Garces *et al.*, 2013; Marchetti *et al.*, 2013), and nonlinear effects will increase with increasing overpressure release rate and supersonic ejection velocities (Needham, 2010). Sustained, broadband infrasonic tremor signals from more sustained eruptions (often described as Vulcanian, sub-Plinian, and Plinian) resemble an infrasonic form of the jet noise produced by smaller scale man-made jets (Matoza *et al.*, 2009, 2013; Fee, Steffke, and Garces, 2010; Fee *et al.*, 2013). Here, for simplicity, we refer to this signal type as volcanic jet noise.

The signals recorded from Sakurajima volcano during the 2013 IAVCEI Volcano Acoustics Workshop (Fee *et al.*, 2014) represent an intermediate case between (1) idealized explosion or blast waves and (2) volcanic jet noise, and they result from explosive processes that are not adequately described by the type eruption styles (e.g., Strombolian, Vulcanian, or sub-Plinian). The explosions at Sakurajima are detailed in the papers by Ishihara (1985), Yokoo *et al.* (2013), and Fee *et al.* (2014); they are characterized by the rapid explosion of a magma plug and consist of strong acoustic waves, ejection of volcanic bombs, and high ash contents. Similar volcanic explosion complexity has been reported elsewhere, where it has been described variously as (a) "small, ballistic and ash-laden eruptive events," e.g., at Karymsky (Johnson, 2007, p. 2); (b) "low-intensity explosions" and "weak Vulcanian," e.g., at Santiaguito and Fuego (Guatemala), Villarrica (Chile), and Stromboli (Italy) (Sahetapy-Engel *et al.*, 2008, p. 1; Marchetti *et al.*, 2009, p. 274); or (c) "ash explosion", e.g., at Karymsky (Firstov *et al.*, 2013, p. 252; Lopez *et al.*, 2013, p. 1). Figures 1 and 2 illustrate selected examples of the Sakurajima workshop infrasound data compared with data from other explosive volcanic eruptions. Many of the Sakurajima signals resemble typical explosion (1) waveforms (Figs. 1d, 2d–f) but with complex onsets and long-duration codas (tens to hundreds of seconds). Other, more sustained Sakurajima signals are qualitatively closer in character to volcanic jet noise (signals 2, Fig. 1e,f) but are not simply a sustained,

doi: 10.1785/0220140110

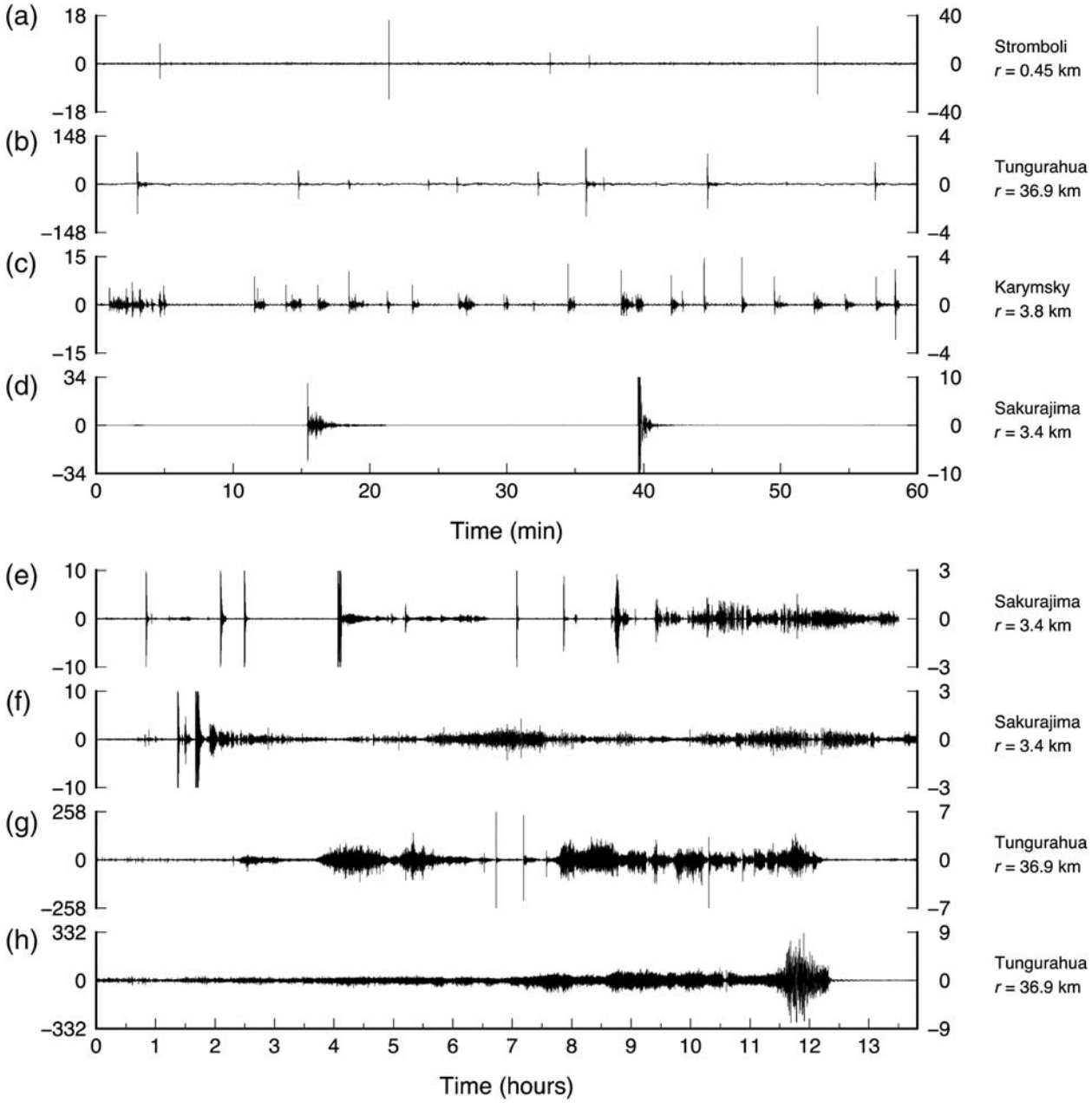

▲ **Figure 1.** Examples of infrasonic pressure waveforms associated with different explosive eruptive styles at different volcanoes. The top four traces (a–d) are of 1-hour duration, whereas the lower four traces (e–h) are of 13.8-hour duration. The labels on the right indicate the volcano and recording distances (range) *r* (in km). In each case, the *y* axis on the right is the observed acoustic pressure amplitude at that range, whereas the *y* axis on the left is the amplitude corrected to a reference distance of 1 km from the source by assuming $1/r$ geometrical spreading for approximate comparison. (a) Typical Strombolian explosions from Stromboli Volcano, Italy (Ripepe and Marchetti, 2002). (b) More energetic but still considered Strombolian explosions from Tungurahua, Ecuador, with codas containing harmonic tremor (Fee, Garces, and Steffke, 2010). (c) Complex explosion waveforms from Karymsky, Kamchatka, with an initial sharp compressional onset followed by short-duration jetting (Lopez *et al.*, 2013) or blow-off (Firstov *et al.*, 2013). (d) Complex explosion waveforms at Sakurajima, similar to those at Karymsky but with longer interevent times and different amplitudes and coda durations. (e) Complex explosion sequence at Sakurajima, including a mix of idealized impulsive explosion waves, volcanic jet noise, and signals of intermediate type. (f) A different Sakurajima example, more akin to volcanic jet noise but with discrete explosions or shocks interspersed. (g) Sub-Plinian eruption from Tungurahua, Ecuador, consisting of multiple sustained sequences of volcanic jet noise interspersed with discrete explosions (Matoza *et al.*, 2009; Fee, Garces, and Steffke, 2010). (h) Sub-Plinian to Plinian eruption at Tungurahua: a sustained volcanic jet noise signal with more gradually evolving signal properties. Panels d, e, and f have been clipped to emphasize lower amplitude explosion codas and jetting; the peak onset compression amplitudes greatly exceed those shown on this plot. This figure is similar to the one appearing in the review paper by Fee and Matoza (2013).

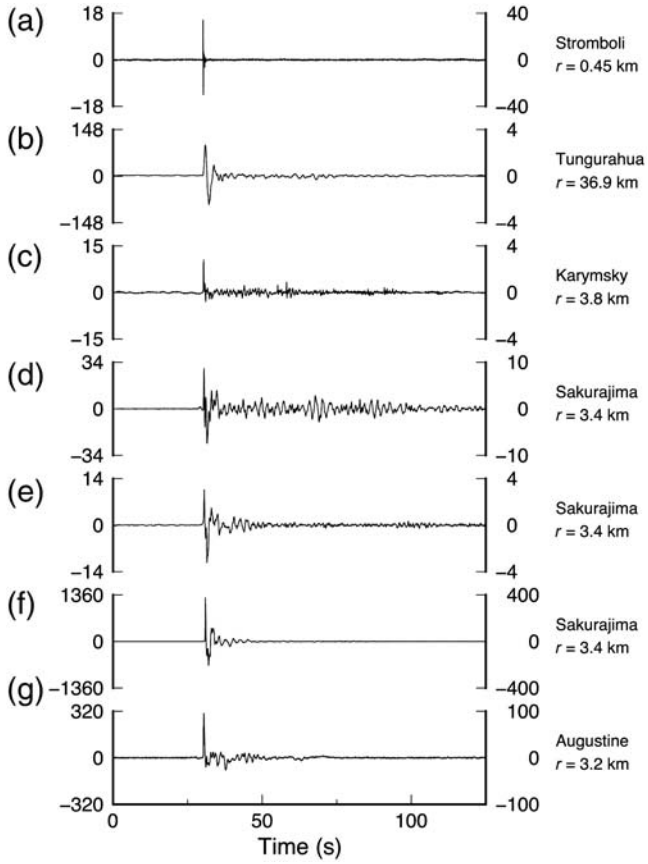

▲ **Figure 2.** Examples of transient infrasonic pressure waveforms from different explosive eruption styles at different volcanoes. See Figure 1 for a detailed figure description. *Y* axes are as described in Figure 1. (a) Strombolian explosion at Stromboli, Italy (Ripepe and Marchetti, 2002). (b) Strombolian explosion at Tungurahua (Fee, Garces, and Steffke, 2010). (c) Complex explosion at Karymsky (Lopez *et al.*, 2013). (d–f) Example complex explosions at Sakurajima. (g) Large Vulcanian explosion from Augustine Volcano, Alaska (Petersen *et al.*, 2006). This figure is similar to the one appearing in the review paper by Fee and Matoza (2013).

smoothly time-varying signal; the signals tend to stop and start erratically. In some cases, a sustained jet-noise-like signal is initiated by a more impulsive explosion (Fig. 1d,e), whereas in other cases the sustained signal begins with an emergent onset (Fig. 1f).

In this paper, we assess the degree of explosion complexity recorded in the 2013 IAVCEI Sakurajima Volcano Acoustics Workshop dataset and in other datasets collected at Karymsky (Lopez *et al.*, 2013) and Tungurahua (Fee, Garces, and Steffke, 2010) volcanoes. These volcanoes exhibit frequent, intermediate-size explosive eruptions with gas and/or ash-rich plumes that are similar in character to explosions from Sakurajima (Fig. 3). For simplicity, we consider only the subset of event types with impulsive onsets (see examples in Figs. 1 and 2). Using these signals, we explore the concept that metrics that are systematically extracted from infrasound data may be used to quantitatively compare and classify explosive eruptive styles at volcanoes. This work is motivated by the observed diversity in explosion styles described above and builds on the previous work by Marchetti *et al.* (2009), Fee, Garces, and Steffke (2010), and Lopez *et al.* (2013). We note the duration of each field campaign is short with respect to the eruptive periods at the target volcanoes; we therefore aim to highlight some of the variability in explosion styles (variability at each volcano and between volcanoes), rather than compile exhaustive explosion catalogs. The large variety in observed infrasonic signals during the short experimental periods at the individual volcanoes (Figs. 1, 2) suggests an immense potential variability in explosive eruptive styles worldwide.

Our results are relevant for using infrasound data to constrain source time functions for plume ascent and ash dispersal models, which has implications for volcanic hazard mitigation. Characterizing variability in explosive eruption infrasound signals (from volcanoes in general) recorded within tens of kilometers from the source is also important for long-range infrasound monitoring of remote explosive volcanism (e.g., Kamo *et al.*, 1994; Fee, Steffke, and Garces, 2010; Dabrowa *et al.*, 2011; Matoza, Le Pichon, *et al.*, 2011; Matoza, Vergoz, *et al.*, 2011), in which the aim is to relate infrasound signal properties, observed at distances of hundreds to thousands of kilometers, to eruption parameters at the source.

DATA PROCESSING

We use the Sakurajima workshop network data collected at stations ARI, HAR, KOM, KUR, and SVO from 18 to 26 July 2013 (Fig. 3a). The data are in MiniSEED format and sampled at 200 Hz, as described by Fee *et al.* (2014). We also use infrasound array datasets collected from 15 to 21 August 2011 at 3.9 km from Karymsky Volcano, Kamchatka, Russia (Fig. 3b) (Lopez *et al.*, 2013) and from 10 to 13 May 2006 at 36.8 km from Tungurahua Volcano, Ecuador (Fig. 3c) (Fee, Garces, and Steffke, 2010). Although the latter two datasets are from arrays, we process them in the same way as the Sakurajima network data to facilitate comparison. The sensors used in the Karymsky experiment clipped at 125 Pa. We seek to characterize explosion complexity by comparing event duration, amplitude, and onset waveform features estimated with an automated method that can be systematically applied to all the data.

Quantifying infrasound waveforms from varied volcanic explosions is challenging. For example, as shown in Figures 1 and 2, explosions at Sakurajima and elsewhere span a large range of amplitudes, and thus the dynamic range of the waveforms complicates the assessment of explosion "coda" duration. Waveforms with large amplitudes in a sharp compressional onset may appear relatively simple when considering the full amplitude range but become more complex and longer duration (coda becomes visible) when considering a reduced amplitude range (see Fig. 1d–f, which employ clipping to show the lower amplitude waveform features). An additional challenge is defining the start and end times of the explosions in sequences (see Fig. 1e,f), in which one event may merge into the next.

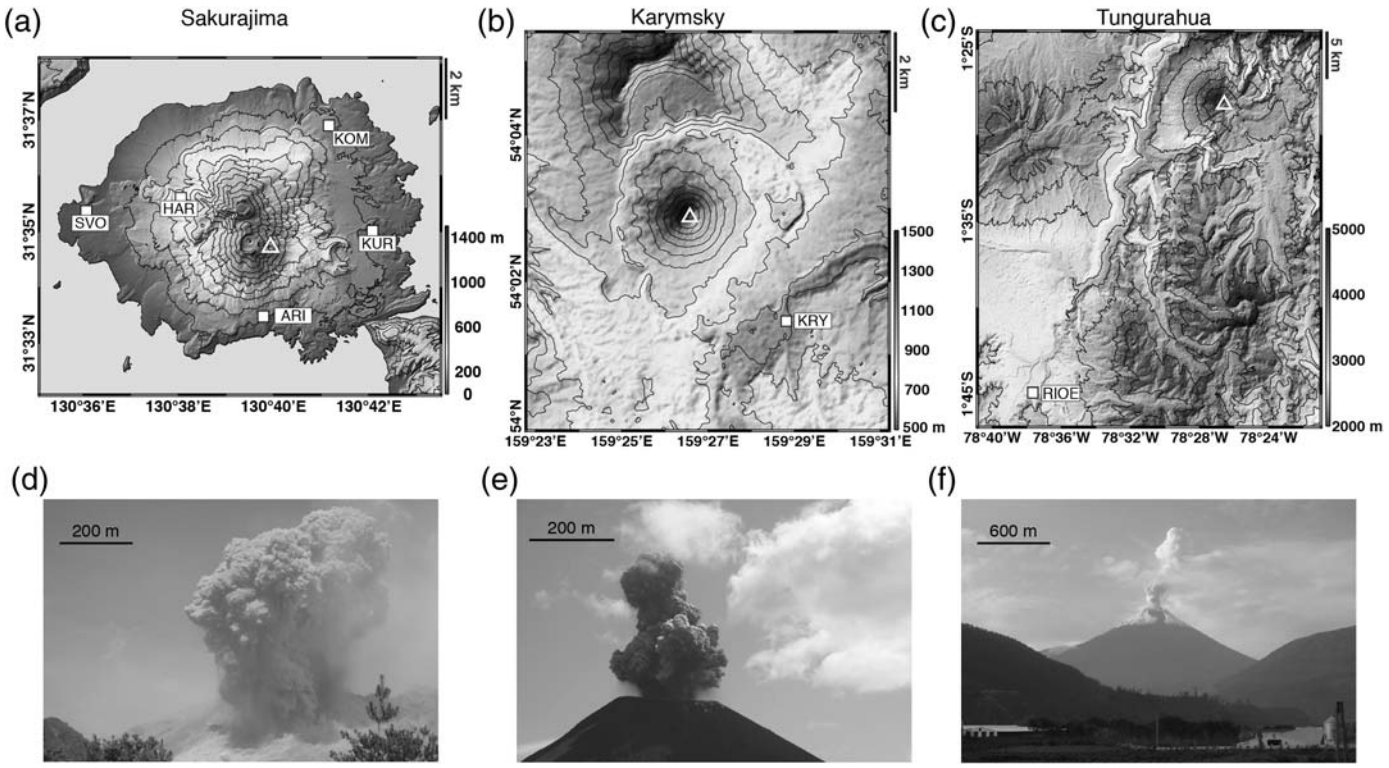

▲ **Figure 3.** (a–c) Location of infrasound sensors (white squares) used in this study at (a) Sakurajima from 18 to 26 July 2013, (b) Karymsky from 15 to 21 August 2011, and (c) Tungurahua from 10 to 13 May 2006. Stations KRY and RIOE are four-element infrasound arrays. White triangles indicate the active vent locations. The contour intervals are (a) 100 m, (b) 100 m, and (c) 500 m. (d–f) Photographs of example explosion events at each volcano. (d) Sakurajima "Vulcanian" explosion. Image courtesy of Jeffrey Johnson, taken at 00:56:19 UTC 21 July 2013 by a camera at station KUR looking west, with timing accuracy of ~1 s. (e) Karymsky low-energy ash explosion (type 1; see Lopez *et al.*, 2013). Image by Sergey Samoylenko, taken at 02:53 UTC 17 August 2011 from ~3.5 km east of Karymsky looking west. (f) Tungurahua small Strombolian gas-rich explosion. Image by David Fee, taken from ~13 km north of Tungurahua.

Because of these challenges, we favor an automated method, which is not subject to analyst bias.

We perform data processing using the ObsPy Python seismic toolbox (Beyreuther *et al.*, 2010). We begin by building catalogs of explosive events (74 events at Sakurajima, 206 events at Karymsky, and 187 events at Tungurahua) using network-coincident recursive short-term average/long-term average (STA/LTA) triggers with an STA length of 0.5 s, an LTA length of 60 s, and a detection threshold of 30 on 0.1–15 Hz band-pass filtered data (Withers *et al.*, 1998; Beyreuther *et al.*, 2010). The network-coincident triggers provide an approximate time for each explosion (Fig. 4). For each event on every station, we re-extract the unfiltered waveform from 100 s before to 3600 s (the maximum allowed event duration) after the coincidence trigger, and we perform further processing to estimate the arrival time, peak pressure, peak acoustic intensity, event duration, acoustic energy of the event onset, acoustic energy of the full event duration, and the peak frequency (Fig. 4). The most difficult parameter to estimate automatically is the event duration, which is sensitive to noise levels before and after the event, pick timing error, and closely spaced events. We use the following methodology to extract infrasound signal metrics of the explosive events (illustrated in Fig. 4).

1. Decimate the data to a 40 Hz sample rate to improve processing speed. This decimation has a negligible effect on the extracted metrics, which are dominated by lower frequencies.
2. Refilter the extracted waveform from 1 to 5 Hz (a consistently high signal-to-noise ratio [SNR] band) and repick it using STA/LTA. Accept the new STA/LTA pick if it falls within (−5 s, 15 s) of the network coincidence trigger; otherwise, retain the network coincidence trigger as the pick. This step provides a more accurate pick of the arrival time on this particular station compared with the network-coincidence trigger (Fig. 4a,c).
3. Estimate the running 5 s time-averaged acoustic intensity $\bar{I} = \bar{p^2}/\rho c$ in W/m^2 for the 1–5 Hz filtered data, in which $\bar{p^2}$ is the mean-square pressure, ρ is the ambient air density (assumed 1.2 kg/m^3), and c is the sound speed (assumed 330 m/s) (Fig. 4b,d).
4. Estimate the event duration τ_d by defining the event end time as when the 1–5 Hz filtered 5 s acoustic intensity drops below a pretrigger value (average of the 5 s intensities in a 25 s window from 35 to 10 s before the pick). The event duration defined in this way is sensitive to 1–5 Hz band noise levels in the pretrigger window. The relatively

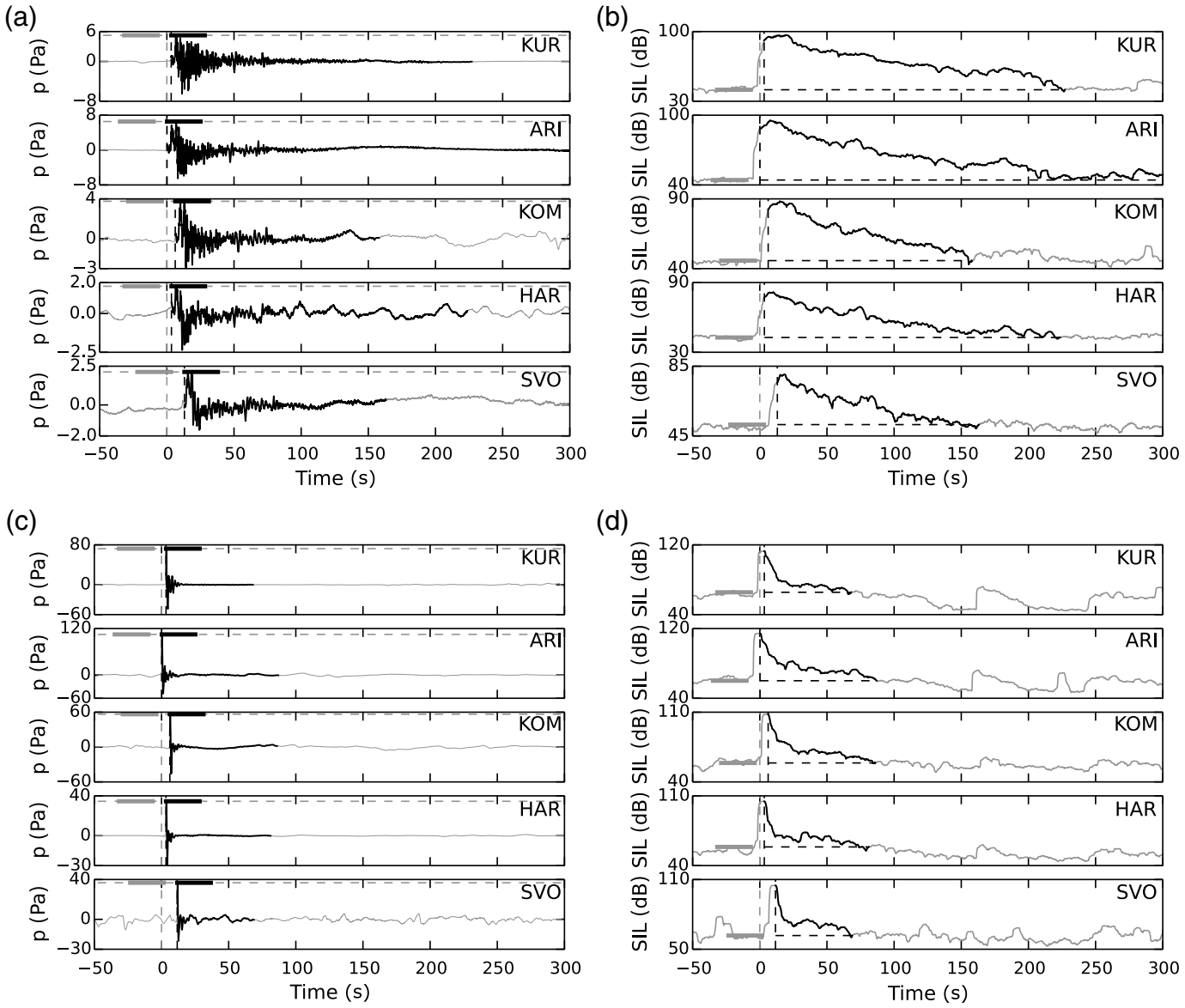

▲ **Figure 4.** Illustration of the metric extraction algorithm applied to (a,b) event 001 and (c,d) event 007 at Sakurajima (see Fig. 5 for event numbers). (a) and (c) The waveform data, decimated to 40 Hz but otherwise unfiltered, are extracted around the network coincidence trigger (vertical dashed gray line at 0 s). The waveforms at each station are then repicked in the 1–5 Hz band to obtain more accurate picks (vertical dashed black lines). The horizontal dashed gray line is the extracted peak pressure in pascals. The thick horizontal gray bar illustrates the time used as a pretrigger noise sample for the event duration and peak frequency estimates. The thick horizontal black bar illustrates the time window used for the peak frequency estimate. (b) and (d) 5 s acoustic intensity values in the 1–5 Hz band, expressed as a sound intensity level (SIL) in decibels relative to 10^{-12} Wm^{-2}. The end of an event duration (black portions of waveforms in all plots) is defined as the time at which the 5 s intensity drops back below the pretrigger (i.e., background) value, represented by the horizontal dashed black line (thick horizontal gray bar illustrates the time window sampled for the pretrigger noise).

narrowband 1–5 Hz filter is only used in steps (1–4) for timing the event arrival times and durations (Fig. 4b,d).

5. Define an event onset duration τ_{onset} as the lesser value of the full event duration and 60 s, which is designed to contain the initial sharp compressional explosive portion of the waveform.
6. Extract the unfiltered peak 5 s acoustic intensity $\bar{I}_{\text{peak}}$ and the maximum peak pressure p_{peak} in pascals for the event onset (see step 5).
7. Estimate the acoustic energy, both for the onset (see step 5) and the full waveform duration (see step 4):

$$E_{\text{event}} = \int_0^{\tau_d} \bar{p^2} dt$$

and

$$E_{\text{onset}} = \int_0^{\tau_{\text{onset}}} \bar{p^2} dt.$$

8. Estimate the onset peak frequency from unfiltered data as follows: Estimate the power spectral density using Welch's method on 25 s noise and signal windows, where the noise window is from 35 to 10 s before the pick and the signal window is from 0 to 25 s after the pick (Fig. 4a,c). The peak frequency is that at which the maximum signal power spectral density occurs, considering only the part of the spectrum >0.2 Hz and where the SNR is greater than 3. The >0.2 Hz cutoff is designed to avoid low-frequency ambient noise (e.g., Bowman *et al.*, 2005).

Our chosen detection parameters were defined based on several randomly chosen explosion events in the databases. We validated the automatic processing results by manually inspecting them against the waveforms (Fig. 4). We performed additional analysis for each automatically defined event, plotting event durations and peak pressures on top of the waveforms (see Figs. 4–7). This step also enabled us to delete a small number of false triggers relating to spurious noise spikes. We also validated the method by evaluating systematic changes and variability in the metrics across the Sakurajima network (see Ⓔ Fig. S1, available in the electronic supplement to this article) and between array elements in the Karymsky and Tungurahua datasets.

The algorithm is intended for events with an impulsive onset and is not designed for emergent signal onsets on tremor or volcanic jet noise (see Fig. 1). Automatically extracting the same set of event metrics for sustained infrasound signals with emergent onsets is better suited to array processing (e.g., Matoza *et al.*, 2007; Fee, Garces, and Steffke, 2010; Matoza, Le Pichon, *et al.*, 2011) and is beyond the scope of the present paper.

RESULTS OF WAVEFORM ANALYSIS: CHARACTERIZING EXPLOSION SIGNAL VARIABILITY

We illustrate the observed waveform variability at Sakurajima, Karymsky, and Tungurahua in Figures 5, 6, and 7, respectively. The events are displayed in increasing order of onset peak pressure (p_{peak}). These figures illustrate how waveform complexity varies with amplitude, with onsets becoming increasingly sharper and cleaner with increasing amplitude. Because these figures show normalized data, the event codas are typically not visible at this scale for the larger amplitude events. However, long event durations indicate the intensities remain above pretrigger values; this is verified by zooming in on the traces (Fig. 1d).

Figures 8 and 9 compare the extracted waveform metrics for the three datasets to better quantify the variability in recorded waveforms at each volcano and between the individual volcanoes. To facilitate approximate comparisons, pressures and energies are scaled for geometric spreading to a reference distance of 1 km, although the usual caveats apply (deviations from the assumed geometrical spreading are expected due to topography and atmospheric propagation effects; e.g., Garces *et al.*, 2013), as highlighted in the Ⓔ electronic supplement. In addition, we found a significant spread in the derived event durations and peak frequencies across the Sakurajima network.

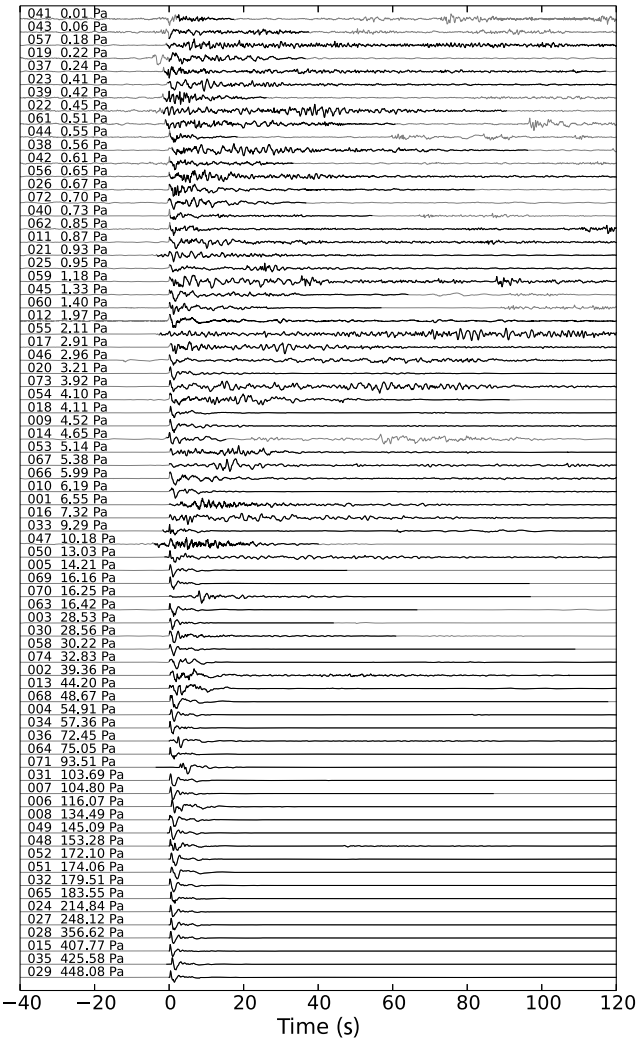

▲ **Figure 5.** Normalized 0.1–15 Hz filtered waveforms for all 74 detected events in the Sakurajima dataset, as recorded at station ARI (range 2.3 km). The labels indicate a unique event number and the onset peak pressure (p_{peak}). The waveforms are shown in increasing order of onset peak pressure (p_{peak}) down the figure. The origin time (0 s) represents the network coincidence trigger for the event, and the event duration is shown as a black line over the raw gray waveform (in many cases the event duration exceeds the plot duration).

This is likely because both of these metrics are sensitive to pretrigger noise, which is variable across the network (see DATA PROCESSING section). Therefore, the event durations and peak frequency values used in Figures 8 and 9 are median averages across all recording stations to make the results more robust with respect to varying SNR at the different stations. In this case, we derive the metrics from each station (or array element) and then take the median. This procedure was developed for the Sakurajima network but also helps with the array element datasets to improve robustness, for example, if an array element is down or mispicked due to a spurious noise burst on that element.

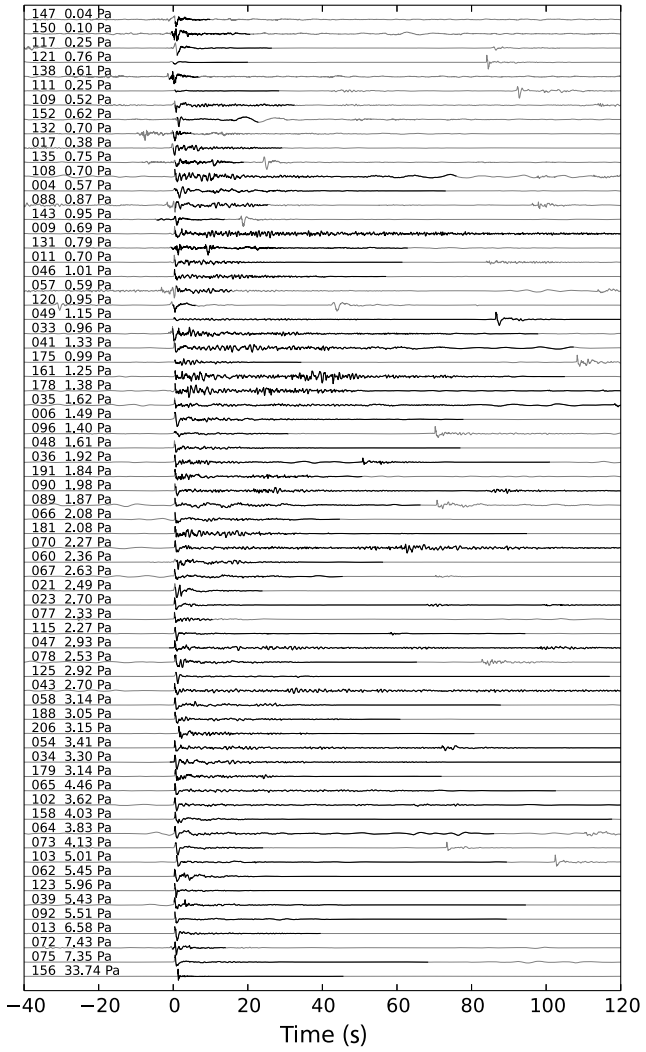

▲ **Figure 6.** As for Figure 5, but for element KRY4 (range 4.0 km) of the Karymsky dataset. For plotting clarity, only 68 of all 206 detected events are shown.

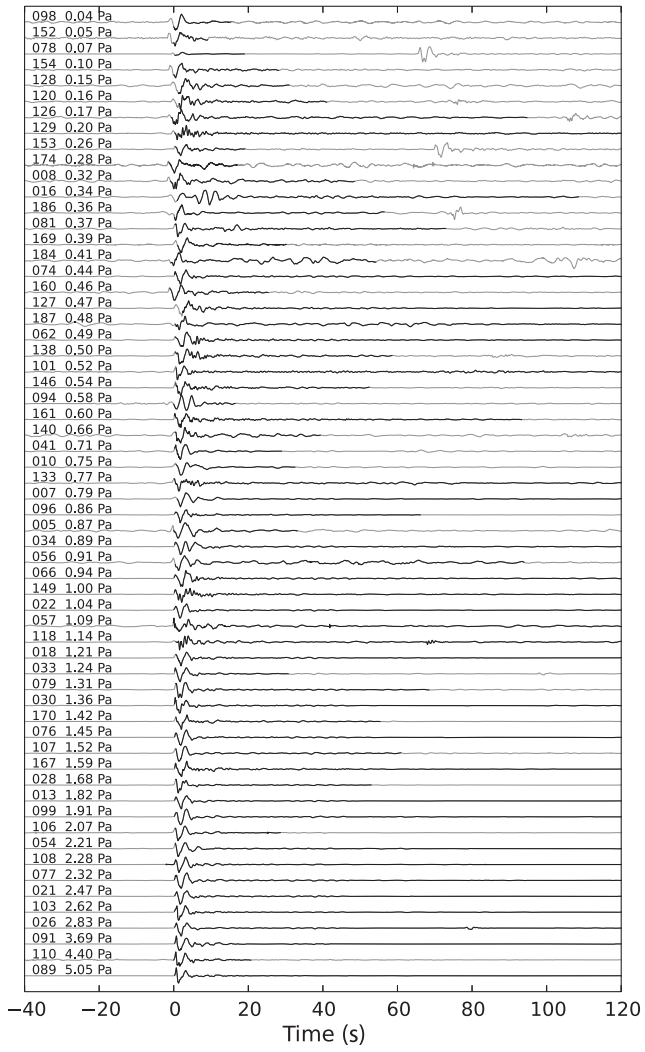

▲ **Figure 7.** As for Figure 5, but for element RIOE1 (range 36.8 km) of the Tungurahua dataset. For plotting clarity, only 61 of all 187 detected events are shown.

Figure 8 illustrates the distributions of individual metrics and clearly shows the higher variability in Sakurajima event intensities, peak pressures, and onset and event energies compared with the other volcanoes during the study periods (see Fig. 8a–d). Given the limited sample sizes of the datasets (data collection periods) and the known variability in eruption style at each of these volcanoes, we cannot extrapolate these observations to consider them representative of the normal behavior of each volcano; rather, they simply capture the variability observed during the particular sampling time. Figures 8e and 8f better quantify the variability in event durations and peak frequencies. There is significant overlap in all metrics between the three volcanoes, making it difficult to separate these event types based on any single metric and highlighting the similarities among the explosions observed from the three volcanoes.

In an attempt to further characterize events, we explore relationships between various infrasound metrics for individual explosions across datasets for all three volcanoes (Fig. 9). We find a general positive correlation between peak pressure and event duration (Fig. 9a), as well as between event energy and event duration (Fig. 9b), although the wide scatter indicates events may occur with different combinations of these parameters (e.g., short duration and large amplitude, short duration and small amplitude, long duration and small amplitude, and long duration and large amplitude). At least two explosions from Karymsky clipped the sensors (pressure amplitude > 125 Pa), plotting near the horizontal dashed line in Figure 9a (the dashed line at 487 Pa represents 125 Pa corrected back to $r = 1$ km); the true values would be somewhere above this line.

We observe a strong positive correlation between onset event energy and peak pressure (Fig. 9c); this is expected because, for impulsive explosions, event onset energy and peak pressure are presumably both dominated by the main sharp compressional onset. It is noteworthy that the Sakurajima events cover the full spread in reduced onset energy versus reduced peak pressure for the other two volcanoes, whereas Karymsky events cluster

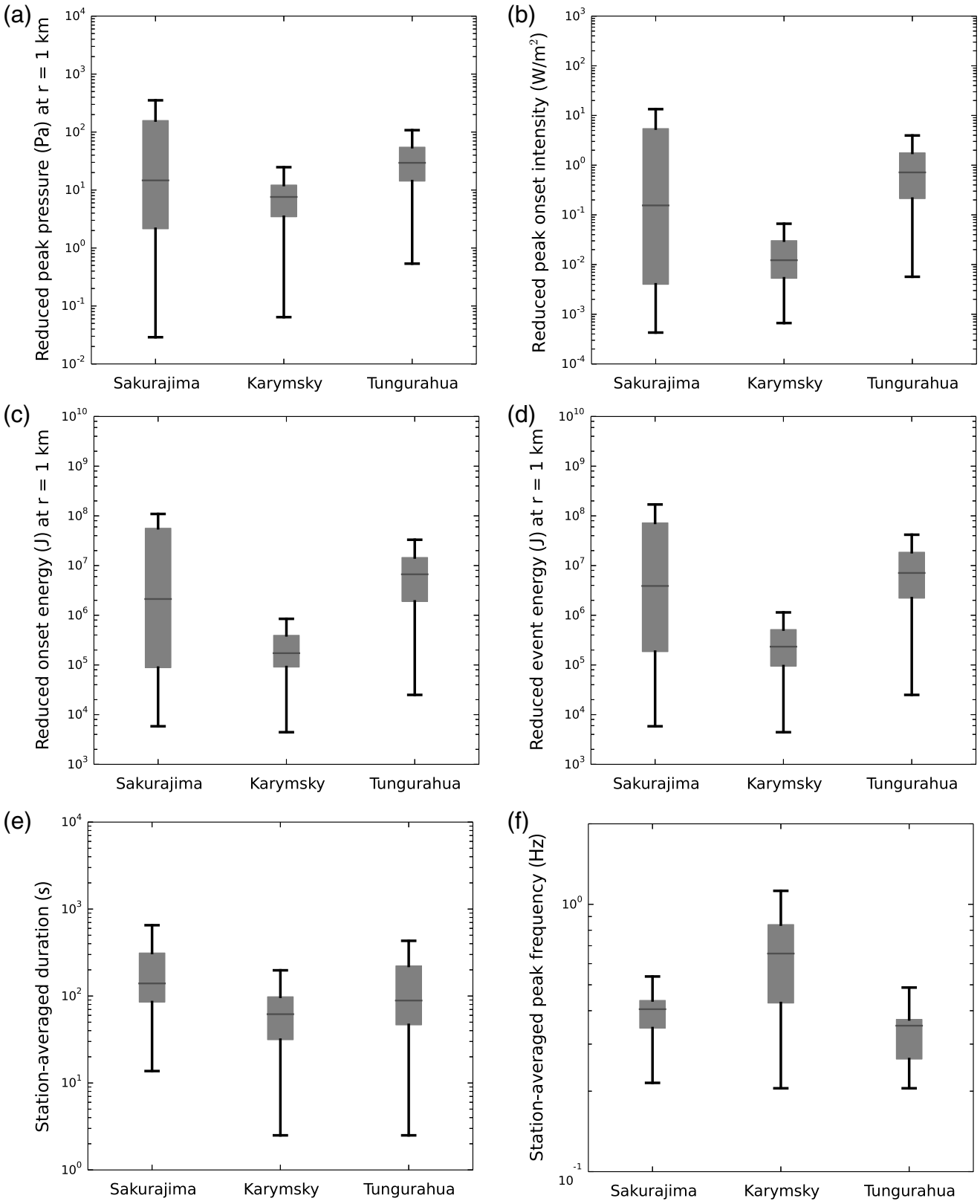

▲ **Figure 8.** Boxplots of infrasound explosion event metrics at the three different volcanoes with dark gray lines at the medians, gray boxes indicating the interquartile range, and black whiskers representing the full data range: (a) reduced peak pressure, (b) reduced peak onset intensity, (c) reduced onset energy, (d) reduced event energy, (e) station-averaged duration, and (f) station-averaged peak frequency. Reduced values assume geometrical spreading to 1 km from the source ($1/r$ in pressure and $1/r^2$ in energy) from values at station ARI (Sakurajima), or from median averages over array elements at Karymsky and Tungurahua.

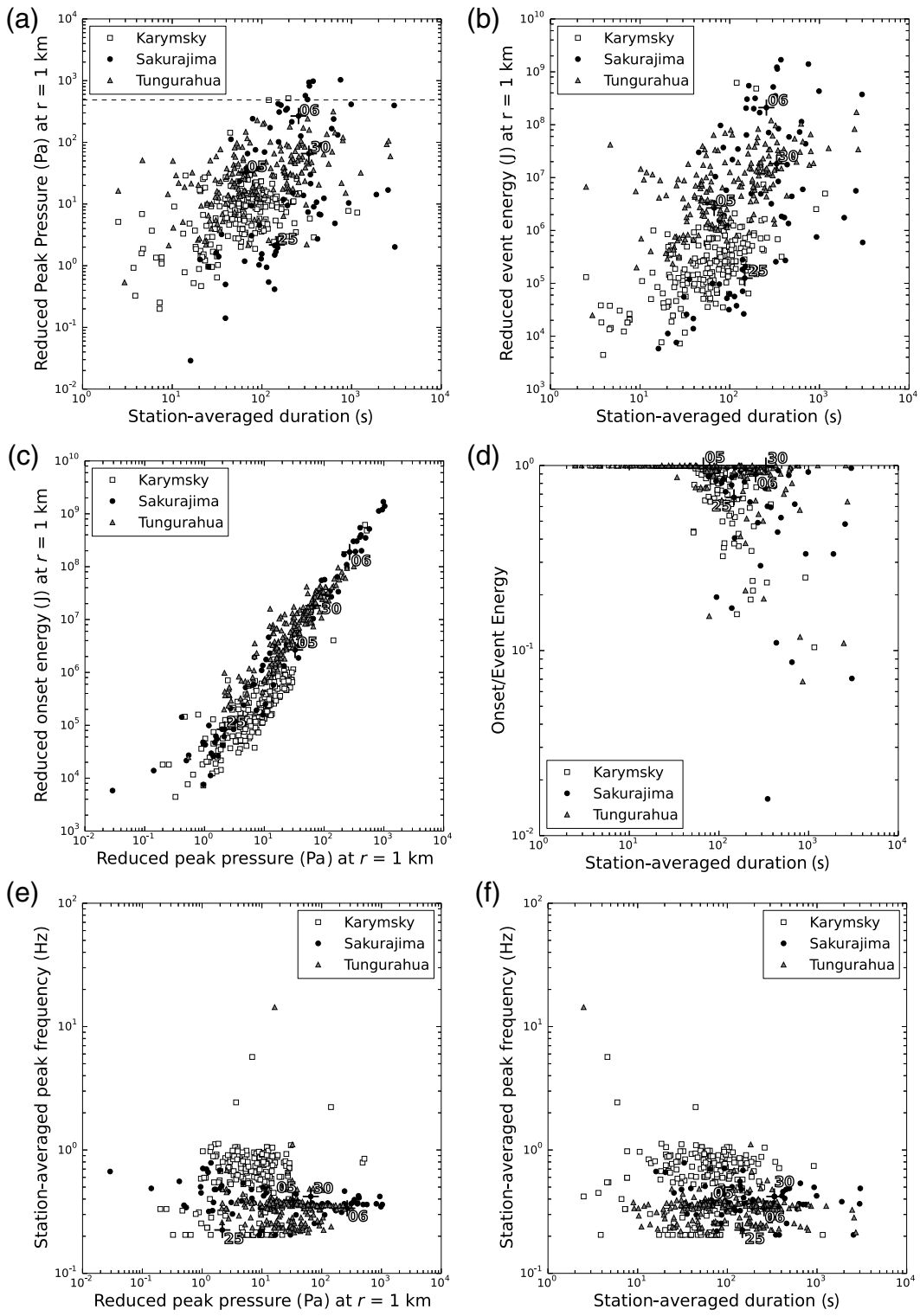

▲ **Figure 9.** Infrasound event metrics compared for the three volcano datasets (Sakurajima, Karymsky, Tungurahua). (a) Reduced peak pressure versus station-averaged event duration. The horizontal dashed line indicates the value at which the sensors used at Karymsky are clipped. (b) Reduced event energy versus station-averaged event duration. (c) Reduced onset energy versus reduced peak pressure. (d) Onset/event energy ratio versus station-averaged duration. (e) Station-averaged peak frequency versus reduced peak pressure. (g) Station-averaged peak frequency versus station-averaged event duration. Reduced values assume geometrical spreading to 1 km from the source using values at station ARI (Sakurajima) or using median averages over array elements at Karymsky and Tungurahua. Energy values (see DATA PROCESSING) are here scaled by $4\pi/\rho c$. On each figure, we identify four events (events 25, 05, 30, and 06) at Sakurajima, which are further highlighted in Figure 10.

with lower energy/pressure and Tungurahua events cluster with higher energy/pressure. Figure 9d shows the ratio of onset energy to total event energy versus the station-averaged event duration. As expected, proportionally more energy is found in the coda for longer duration events. However, we note that, by definition, $E_{onset} = E_{event}$ for events with $\tau_d \leq 60$ s, which results in many events having $E_{onset}/E_{event} = 1$. We also compare event peak frequency with peak pressure (Fig. 9e) and event duration (Fig. 9f). We observe some clustering in these parameter spaces, indicating that frequency content is one of the most useful metrics for separating and classifying event variability. Specifically, waveforms at Tungurahua tend to occur with a preferred peak frequency between 0.3 and 0.4 Hz, Karymsky signals generally have higher peak frequencies than the other volcanoes (primarily ranging from ~0.4–1 Hz and with the greatest scatter in peak frequency), and Sakurajima explosions are also somewhat clustered with peak frequencies of 0.3–0.5 Hz (note the > 0.2 Hz cutoff in this metric).

DISCUSSION

In most cases, we find only weak correlations and/or minor clustering in the infrasound signal metric parameter spaces (Fig. 9). These observations highlight the inherent complexity and variability in explosion styles exhibited at individual volcanoes, as well as the bulk similarities in overall explosion character observed at three geographically dispersed volcanoes. The relationship between infrasound and explosion character is further illustrated in Figure 10, which shows visual observations of explosions at Sakurajima along with the corresponding infrasound waveforms; the associated metrics are highlighted in Figure 9. The four explosions exhibit visual differences in eruptive intensity (e.g., plume ascent rate, volume of erupted material) with corresponding differences in the waveforms and metrics. For example, event 25 (Fig. 10a) has low peak pressure and onset energy, it erupts less material according to its smaller apparent plume volume, and its plume rise rate is slower than for event 6, which is both acoustically and visually a more energetic explosion. Other fine-scale waveform features (not captured in the simple metrics) contain additional information about the eruptive processes. For example, event 30 (Fig. 10c) initiates as two distinct ash expansions, with an associated double blast seen in the infrasound waveform. Future work could explore the physical parameters controlling both the explosion style and the location of the associated acoustic signals in the feature spaces shown in Figure 9 (e.g., Bowman *et al.*, 2014). These parameters may include the preblast overpressure, rate of pressure release, explosion initiation (burial) depth, mechanical strength of the overburden, fracture density, and volume of material available to erupt.

We obtain an unexpected relationship between event amplitude and event duration (Figs. 5–7, 9a,b). Before beginning our data analysis, we had originally hypothesized that explosions with larger amplitude would have shorter durations than those with smaller amplitude, that is, peak pressure would vary inversely with event duration. This is because we were expecting the simplest explosion or blast waveforms (Marchetti *et al.*, 2013) would have high amplitudes and very short durations, whereas smaller events would tend to be more sustained degassing events. These figures show that, on the contrary, even large-amplitude explosion events tend to have long-duration codas, consistent with visual observations of sustained gas and/or ash venting following the initial sharp compressional onset at all three volcanoes. These long durations are too long to attribute to reverberation and scattering from topography. This highlights the complexity in explosion mechanisms at intermediate composition (andesitic) volcanoes. The source mechanism associated with sustained gas and/or ash venting likely departs significantly from a monopole approximation (Woulff and McGetchin, 1976; Matoza *et al.*, 2013).

Our observations suggest that the emission style (ash rich versus gas rich) could potentially be identified via careful analyses of infrasound waveform amplitude and frequency content. The data shown in Figure 9c indicate the sampled Sakurajima events exhibit a greater variety in event amplitudes and that the Tungurahua events generally have higher amplitudes than the Karymsky events. Although there is uncertainty related to the geometrical spreading correction, the Tungurahua explosions were gas rich and ash poor (Fee, Garces, and Steffke, 2010), whereas the Karymsky events were more ash rich (Lopez *et al.*, 2013). We may expect gas-dominated explosions to have more explosive energy than ash-dominated ones, due to the large volume increase of gas under depressurization (Sparks *et al.*, 1997). We note that the overall similarity of waveform features and signal metrics between the gas-rich explosions at Tungurahua and more ash-rich explosions at Karymsky and Sakurajima highlights the difficulty in trying to identify ash release based on simple metrics extracted from infrasound data. However, Figures 5–7 and 9e,f suggest that more detailed waveform and frequency feature extraction may be able to achieve this. The clustering of peak frequencies at different values for the different volcanoes (Fig. 9e,f) may also indicate a vent geometry effect.

This work is preliminary, and these datasets represent tiny windows into the possible explosion variability throughout the eruptive and geological lifespans of these three volcanoes. We expect folding in data from other volcanoes around the world would illustrate much greater variability. These considerations underscore the importance of long-term volcano acoustic datasets, as exemplified by the long-term measurements of infrasound at the Sakurajima Volcano Observatory. This type of investigation would also benefit from greater data availability through sharing multiple community datasets from different volcanoes, permitting systematic comparisons among volcanoes.

CONCLUSIONS

We performed automated waveform processing on three volcano infrasound datasets, extracting signal metrics for 74 events from 18 to 26 July 2013 at Sakurajima, 206 events from 15 to 21 August 2011 at Karymsky, and 187 events from 10 to 13 May 2006 at Tungurahua. Our results permit systematic

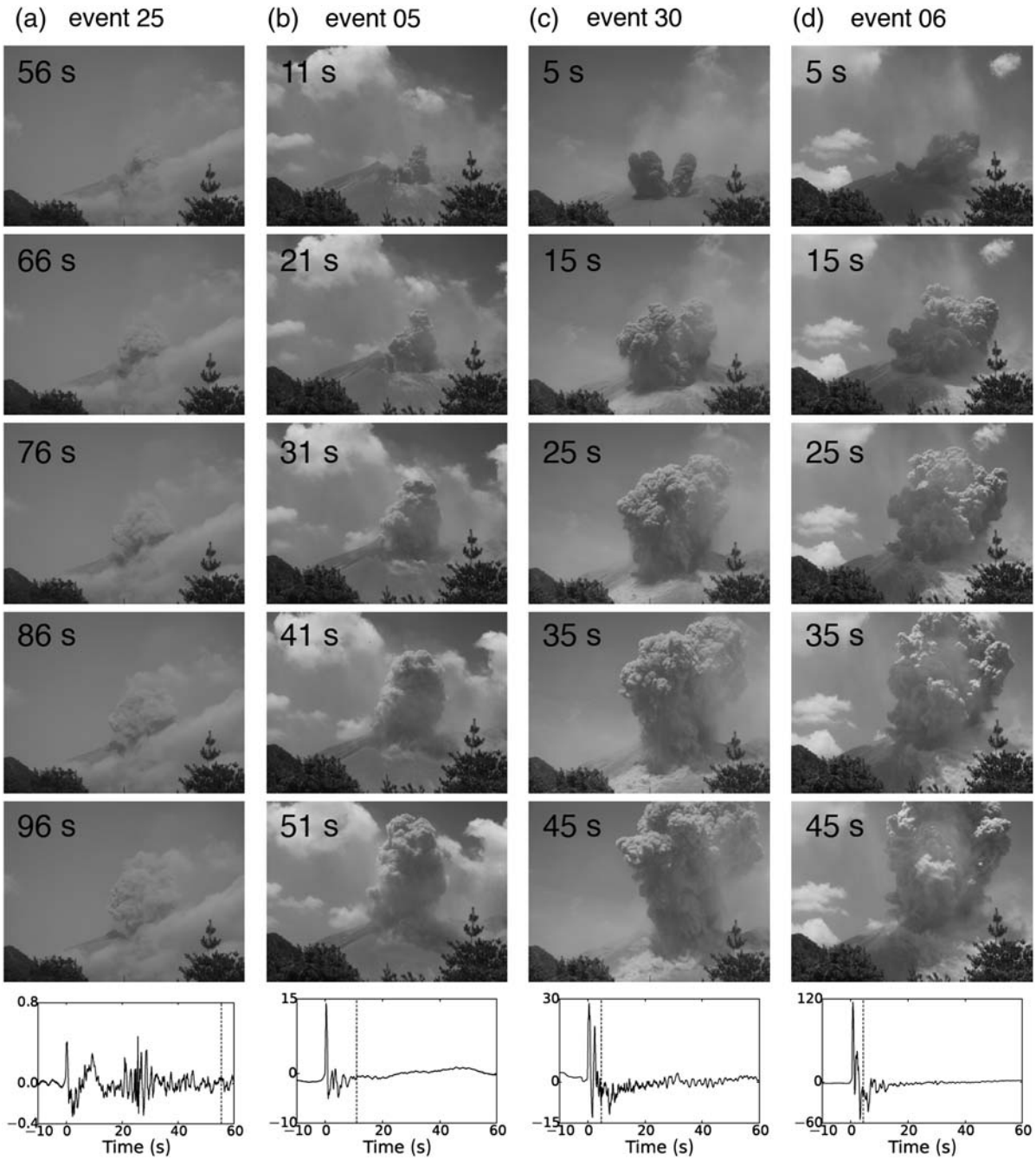

▲ **Figure 10.** Comparison of image sequences and infrasound waveforms for four Sakurajima explosions spanning a range of peak pressures (see Fig. 9). Photographs were collected automatically at station KUR (courtesy of Jeffrey Johnson) and infrasound waveforms are at station ARI. Each column represents an image sequence in 10 s snapshots, beginning at the time indicated by the vertical dashed line on the lower waveform figure. The dashed line position on the waveform is estimated by adding the infrasound propagation time (from the source to station ARI, assuming 330 m/s) to the first image capture time to simulate that the waveform is capturing the explosion process without the propagation delay. The labels in the upper-left corner refer each image to the waveform origin time, again corrected for propagation (the first labeled snapshot time is the time of the dashed line). Note that the main infrasound explosive compression occurs prior to the first snapshot time shown in all cases, as there is a delay between explosion initiation and the visible appearance of tephra. The waveform plot origin times ($t = 0$ s on the x axis) in UTC are as follows: (a) 21:43:06.460 on 20 July 2013, (b) 02:44:38.025 on 19 July 2013, (c) 00:55:55.275 on 21 July 2013, and (d) 03:04:46.465 on 19 July 2013. Y scales in the waveforms are pressure in pascals. All waveforms are unfiltered to show the positively skewed, blast-like nature of the waveforms (Marchetti *et al.*, 2013), except (a), which is filtered from 0.05 to 15 Hz to reduce wind and cultural noise. Note the double-peaked blast waveform in (c), corresponding to two explosive emissions. We chose the image sequence in (a) to begin later in the waveform compared with the other examples because of the slow plume rise time in this event.

comparisons of volcano infrasound waveform variability associated with a range of volcanic explosion styles. Waveforms recorded in the three volcano datasets are complex in character and vary between idealized end members of short-duration explosion waves and long-duration jetting; we designed an automated algorithm to characterize variability in the shorter-duration transient set (events beginning with an impulsive onset, considering a maximum event duration of 1 hour). Such waveforms appear to be a characteristic feature and behavior of intermediate-composition (andesitic) low-level explosive volcanism. Extracted signal metrics such as event duration, peak pressure, peak acoustic intensity, and peak frequency exhibit differences between the three datasets, but overall this type of behavior produces a similar range of acoustic signal properties at the three volcanoes considered.

Other physical eruption styles not considered in our automated analysis in the present study, such as sustained Plinian eruptions, will likely have very different values of extracted signal metrics (e.g., event duration), thus providing a potential basis for automatically identifying bulk properties of the physical eruption style based on simple infrasound metrics. However, the results of this study demonstrate that a great variety of explosion styles and flow behaviors can produce relatively similar bulk acoustic waveform properties, indicating that a finer scale classification of physical eruptive styles requires more advanced field studies, waveform analyses, and modeling. For example, we find that tephra-rich and gas-rich (tephra poor) explosions produce quite similar waveform metrics, which would make it challenging to automatically determine ash content based on simple metrics extracted from sparse long-range infrasound data. However, with more local volcano monitoring and dedicated field studies, it may be possible to identify unique waveform properties associated with ash-rich or ash-poor eruptions (e.g., Ripepe and Marchetti, 2002; Lopez *et al.*, 2013). Detailed field studies and infrasound waveform modeling, combined with laboratory and numerical studies, may provide eruption velocity source time functions for this class of low-intensity explosive eruptions, constraining the dynamics of plume ascent and ash dispersal from unsteady eruptions and helping to mitigate societal and economic volcanic hazards.

ACKNOWLEDGMENTS

We thank Jeffrey Johnson for collecting and providing the image data used in Figure 10, Maurizio Ripepe for providing the Stromboli data used in Figures 1 and 2, and Kirsten Chojnicki for discussions. We are grateful to SVO, KBGS/IVS, and IGEPN for field and logistical support with the data collection. We thank two anonymous reviewers for helping us to improve the manuscript. We used ASTER digital elevation model (DEM) data in Figure 3. R.S.M. acknowledges support from the Cecil H. and Ida M. Green Foundation at the Institute of Geophysics and Planetary Physics, Scripps Institution of Oceanography, and National Science Foundation (NSF) Grant EAR-1113338. D.F. acknowledges support from the Geophysical Institute and NSF Grant EAR-1331084. T.M.L. acknowledges support from the Geophysical Institute, the Alaska Space Grant Consortium, and NSF Grant EAR-1250148.

REFERENCES

Beyreuther, M., R. Barsch, L. Krischer, T. Megies, Y. Behr, and J. Wassermann (2010). ObsPy: A Python toolbox for seismology, *Seismol. Res. Lett.* **81,** no. 3, 530–533.

Bowman, J. R., G. E. Baker, and M. Bahavar (2005). Ambient infrasound noise, *Geophys. Res. Lett.* **32,** L09803, doi: 10.1029/2005GL022486.

Bowman, D. C., J. Taddeucci, K. Kim, J. F. Anderson, J. M. Lees, A. H. Graettinger, I. Sonder, and G. A. Valentine (2014). The acoustic signatures of ground acceleration, gas expansion, and spall fallback in experimental volcanic explosions, *Geophys. Res. Lett.* **41,** 1916–1922.

Caplan-Auerbach, J., A. Bellesiles, and J. K. Fernandes (2010). Estimates of eruption velocity and plume height from infrasonic recordings of the 2006 eruption of Augustine Volcano, Alaska, *J. Volcanol. Geoth. Res.* **189,** no. 1, 12–18.

Dabrowa, A. L., D. N. Green, A. C. Rust, and J. C. Phillips (2011). A global study of volcanic infrasound characteristics and the potential for long-range monitoring, *Earth Planet. Sci. Lett.* **310,** no. 3, 369–379.

Delle Donne, D., and M. Ripepe (2012). High-frame rate thermal imagery of Strombolian explosions: Implications for explosive and infrasonic source dynamics, *J. Geophys. Res.* **117,** B09206, doi: 10.1029/2011JB008987.

Fee, D., and R. S. Matoza (2013). An overview of volcano infrasound: From Hawaiian to Plinian, local to global, *J. Volcanol. Geoth. Res.* **249,** 123–139.

Fee, D., M. Garces, and A. Steffke (2010). Infrasound from Tungurahua Volcano 2006–2008: Strombolian to Plinian eruptive activity, *J. Volcanol. Geoth. Res.* **193,** no. 1, 67–81.

Fee, D., R. S. Matoza, K. L. Gee, T. B. Neilsen, and D. E. Ogden (2013). Infrasonic crackle and supersonic jet noise from the eruption of Nabro Volcano, Eritrea, *Geophys. Res. Lett.* **40,** no. 16, 4199–4203.

Fee, D., A. Steffke, and M. Garces (2010). Characterization of the 2008 Kasatochi and Okmok eruptions using remote infrasound arrays, *J. Geophys. Res.* **115,** D00L10, doi: 10.1029/2009JD013621.

Fee, D., A. Yokoo, and J. B. Johnson (2014). Introduction to an open community infrasound dataset from the actively erupting Sakurajima Volcano, Japan, *Seismol. Res. Lett.* **85,** no. 6, doi: 10.1785/0220140051.

Firstov, P. P., and N. M. Kravchenko (1996). Estimation of the amount of explosive gas released in volcanic eruptions using air waves, *Volcanol. Seismol.* **17,** 547–560.

Firstov, P. P., D. Fee, and E. R. Makhmudov (2013). The explosive activity of Karymskii Volcano, Kamchatka: Acoustic and seismic observations, *J. Volcanol. Seismol.* **7,** no. 4, 252–264.

Garces, M. A., D. Fee, and R. Matoza (2013). Volcano acoustics, in *Modeling Volcanic Processes: The Physics and Mathematics of Volcanism*, Chapter 16, S. A. Fagents, T. K. P. Gregg, and R. M. C. Lopes (Editors), Cambridge University Press, New York.

Ishihara, K. (1985). Dynamical analysis of volcanic explosion, *J. Geodyn.* **3,** 327–349, doi: 10.1016/0264-3707(85)90041-9.

Johnson, J. B. (2003). Generation and propagation of infrasonic airwaves from volcanic explosions, *J. Volcanol. Geoth. Res.* **121,** no. 1, 1–14.

Johnson, J. B. (2007). On the relation between infrasound, seismicity, and small pyroclastic explosions at Karymsky Volcano, *J. Geophys. Res.* **112,** B08203, doi: 10.1029/2006JB004654.

Johnson, J. B., and A. J. C. Miller (2014). Application of the monopole source to quantify explosive flux during vulcanian explosions at Sakurajima Volcano (Japan), *Seismol. Res. Lett.* **85,** no. 6, doi: 10.1785/0220140058.

Johnson, J. B., and M. Ripepe (2011). Volcano infrasound: A review, *J. Volcanol. Geoth. Res.* **206,** no. 3, 61–69.

Kamo, K., K. Ishihara, and M. Tahira (1994). Infrasonic and seismic detection of explosive eruptions at Sakurajima Volcano, Japan, and the PEGASAS-VE early-warning system, in *Proc. of the First International Symposium on Volcanic Ash and Aviation Safety*, *U.S. Geol. Surv. Bull.*, Seattle, Washington, July 1991, Vol. 2047, 357–365.

Lopez, T., D. Fee, F. Prata, and J. Dehn (2013). Characterization and interpretation of volcanic activity at Karymsky Volcano, Kamchatka, Russia, using observations of infrasound, volcanic emissions, and thermal imagery, *Geochem. Geophys. Geosyst.* **14,** no. 12, 5106–5127.

Marchetti, E., M. Ripepe, D. Delle Donne, R. Genco, A. Finizola, and E. Garaebiti (2013). Blast waves from violent explosive activity at Yasur Volcano, Vanuatu, *Geophys. Res. Lett.* **40,** no. 22, 5838–5843.

Marchetti, E., M. Ripepe, A. J. L. Harris, and D. Delle Donne (2009). Tracing the differences between Vulcanian and Strombolian explosions using infrasonic and thermal radiation energy, *Earth Planet. Sci. Lett.* **279,** no. 3, 273–281.

Matoza, R. S., D. Fee, M. A. Garcés, J. M. Seiner, P. A. Ramon, and M. A. H. Hedlin (2009). Infrasonic jet noise from volcanic eruptions, *Geophys. Res. Lett.* **36,** no. L08303, doi: 10.1029/2008GL036486.

Matoza, R. S., D. Fee, T. B. Neilsen, K. L. Gee, and D. E. Ogden (2013). Aeroacoustics of volcanic jets: Acoustic power estimation and jet velocity dependence, *J. Geophys. Res.* **118,** no. 12, 6269–6284.

Matoza, R. S., M. A. Hedlin, and M. A. Garcés (2007). An infrasound array study of Mount St. Helens, *J. Volcanol. Geoth. Res.* **160,** no. 3, 249–262.

Matoza, R. S., A. Le Pichon, J. Vergoz, P. Herry, J. Lalande, H. Lee, I. Che, and A. Rybin (2011). Infrasonic observations of the June 2009 Sarychev Peak eruption, Kuril Islands: Implications for infrasonic monitoring of remote explosive volcanism, *J. Volcanol. Geoth. Res.* **200,** 35–48.

Matoza, R. S., J. Vergoz, A. Le Pichon, L. Ceranna, D. N. Green, L. G. Evers, M. Ripepe, P. Campus, L. Liszka, T. Kvaerna, E. Kjartansson, and A. Hoskuldsson (2011). Long-range acoustic observations of the Eyjafjallajökull eruption, Iceland, April–May 2010, *Geophys. Res. Lett.* **38,** L06308, doi: 10.1029/2011GL047019.

Needham, C. E. (2010). *Blast Wave Propagation*, Springer, Berlin, Germany, 87–99.

Petersen, T., S. De Angelis, G. Tytgat, and S. R. McNutt (2006). Local infrasound observations of large ash explosions at Augustine Volcano, Alaska, during January 11–28, 2006, *Geophys. Res. Lett.* **33,** L12303, doi:10.1029/2006GL026491.

Ripepe, M., and E. Marchetti (2002). Array tracking of infrasonic sources at Stromboli Volcano, *Geophys. Res. Lett.* **29,** no. 22, 33-1–33-4.

Sahetapy-Engel, S. T., A. J. Harris, and E. Marchetti (2008). Thermal, seismic and infrasound observations of persistent explosive activity and conduit dynamics at Santiaguito lava dome, Guatemala, *J. Volcanol. Geoth. Res.* **173,** no. 1, 1–14.

Sparks, R. S. J., M. I. Bursik, S. N. Carey, J. Gilbert, L. S. Glaze, H. Sigurdsson, and A. W. Woods (1997). *Volcanic Plumes*, Wiley, Chichester.

Vergniolle, S., and J. Caplan-Auerbach (2006). Basaltic thermals and Subplinian plumes: Constraints from acoustic measurements at Shishaldin Volcano, Alaska, *Bull. Volcanol.* **68,** nos. 7/8, 611–630.

Walker, G. P. (1973). Explosive volcanic eruptions—A new classification scheme, *Geologische Rundschau* **62,** no. 2, 431–446.

Withers, M., R. Aster, C. Young, J. Beiriger, M. Harris, S. Moore, and J. Trujillo (1998). A comparison of select trigger algorithms for automated global seismic phase and event detection, *Bull. Seismol. Soc. Am.* **88,** no. 1, 95–106.

Woulff, G., and T. R. McGetchin (1976). Acoustic noise from volcanoes: Theory and experiment, *Geophys. J. Roy. Astron. Soc.* **45,** no. 3, 601–616.

Yokoo, A., and K. Ishihara (2007). Analysis of pressure waves observed in Sakurajima eruption movies, *Earth Planets Space* **59,** no. 3, 177–181.

Yokoo, A., M. Iguchi, T. Tameguri, and K. Yamamato (2013). Processes prior to outbursts of Vulcanian eruption at Showa crater of Sakurajima Volcano, *Bull. Volcanol. Soc. Jpn.* **58,** 163–181.

Robin S. Matoza
Institute of Geophysics and Planetary Physics
Scripps Institution of Oceanography
University of California, San Diego
La Jolla, California 92093-0225 U.S.A.
rmatoza@ucsd.edu

David Fee[1]
Taryn M. López
Geophysical Institute
Alaska Volcano Observatory
University of Alaska Fairbanks
903 Koyukuk Drive
Fairbanks, Alaska 99775 U.S.A.

Published Online 15 October 2014

[1] Also at Geophysical Institute, Wilson Infrasound Observatories, University of Alaska Fairbanks, 903 Koyukuk Drive, Fairbanks, Alaska 99775 U.S.A.